Published in final edited form as:
Biol Cybern. 2011 March ; 104(3): 209–223. doi:10.1007/s00422-011-0428-8.

A rapid form of activity-dependent recovery from short-term synaptic depression in the intensity pathway of the auditory brainstem

Katrina M. MacLeod and
Department of Biology, University of Maryland, College Park, MD 20742, USA, macleod@umd.edu

Neuroscience and Cognitive Science Program, University of Maryland, College Park, MD 20742, USA

Timothy K. Horiuchi
Department of Electrical and Computer Engineering, The Institute for Systems Research, University of Maryland, College Park, MD 20742, USA

Neuroscience and Cognitive Science Program, University of Maryland, College Park, MD 20742, USA

Abstract

Short-term synaptic plasticity acts as a time- and firing rate-dependent filter that mediates the transmission of information across synapses. In the avian auditory brainstem, specific forms of plasticity are expressed at different terminals of the same auditory nerve fibers and contribute to the divergence of acoustic timing and intensity information. To identify key differences in the plasticity properties, we made patch-clamp recordings from neurons in the cochlear nucleus responsible for intensity coding, nucleus angularis, and measured the time course of the recovery of excitatory postsynaptic currents following short-term synaptic depression. These synaptic responses showed a very rapid recovery, following a bi-exponential time course with a fast time constant of ~40 ms and a dependence on the presynaptic activity levels, resulting in a crossing over of the recovery trajectories following high-rate versus low-rate stimulation trains. We also show that the recorded recovery in the intensity pathway differs from similar recordings in the timing pathway, specifically the cochlear nucleus magnocellularis, in two ways: (1) a fast recovery that was not due to recovery from postsynaptic receptor desensitization and (2) a recovery trajectory that was characterized by a non-monotonic bump that may be due in part to facilitation mechanisms more prevalent in the intensity pathway. We tested whether a previously proposed model of synaptic transmission based on vesicle depletion and sequential steps of vesicle replenishment could account for the recovery responses, and found it was insufficient, suggesting an activity-dependent feedback mechanism is present. We propose that the rapid recovery following depression allows improved coding of natural auditory signals that often consist of sound bursts separated by short gaps.

Correspondence to: Katrina M. MacLeod.

Electronic supplementary material The online version of this article (doi:10.1007/s00422-011-0428-8) contains supplementary material, which is available to authorized users.

Keywords

Auditory nerve; Cochlear nucleus; Angularis; Magnocellularis; Short-term depression; Short-term facilitation; Vesicle cycling

1 Introduction

The rapid, activity-dependent alteration of the strength of synapses, known as short-term synaptic plasticity, contributes to neural coding by acting as a filter through which the information contained in the presynaptic spike train must pass (O'Donovan and Rinzel 1997; Markram et al. 1998; Schneggenburger et al. 2002; Trussell 2002; von Gersdorff and Borst 2002; Abbott and Regehr 2004; Blitz et al. 2004). Synapses that differ in the specific time- and activity-dependence of their filtering properties process information differently, such that the same presynaptic spike train can drive multiple postsynaptic targets differently. The auditory brainstem contains circuits with a rich diversity of functionality, offering an opportunity to relate short-term plasticity to specific sensory transformations. We investigated the short-term plasticity in the avian cochlear nuclei, the first relays of auditory information arriving via the auditory nerve. Numerous well-studied morphological and intrinsic properties distinguish the parallel neural pathways that encode timing and intensity information (Oertel 1999; Trussell 1999).

Recently, short-term synaptic plasticity has been proposed to be another distinguishing property between the two pathways (MacLeod and Carr 2007; MacLeod et al. 2007; Cao et al. 2008). In the avian cochlear nucleus involved in the intensity pathway, nucleus angularis (NA), nerve terminals exhibit a mixture of short-term synaptic facilitation and depression that allows the transmission of rate-encoded intensity information important for interaural level difference coding (MacLeod et al. 2007). In contrast, in the avian cochlear nucleus involved in the timing pathway, nucleus magnocellularis (NM), nerve terminals exhibit pronounced short-term synaptic depression. Similar depression in the second-order timing nucleus, nucleus laminaris (NL) acts as a synaptic gain control mechanism that contributes to intensity-invariant coding of interaural timing differences (Trussell 1999; Kuba et al. 2002; Cook et al. 2003). This represents a rare occasion in which the short-term plasticity properties can be clearly linked to a well-understood functional dichotomy.

In order to further refine our understanding of how plasticity differs in the two pathways, we investigate the kinetics of the recovery from short-term depression in the two cochlear nuclei NA and NM. The overall reduced depression at synapses in NA compared to NM may be explained by a number of possible mechanisms. At the presynaptic level, there may be a lower initial probability of vesicle release, more rapid rate of replenishment of synaptic vesicles (either basal or activity-dependent) or presynaptic facilitation may offset the depression. Postsynaptically, auditory nerve synapses in NA may evoke less receptor desensitization than seen at NM synapses (Brenowitz and Trussell 2001a). Since individual auditory nerve axons bifurcate to send one branch to each of the cochlear nuclei, any differences in the presynaptic properties provide insight into the target-specific regulation of synaptic plasticity.

Short-term depression is often attributed to the depletion of synaptic vesicles at the active zone and thus a key operating parameter is the rate of vesicle replenishment. A rapid component of recovery from depression has been reported at several specialized auditory pathway synapses, including the endbulb synapses in the auditory brainstem and hair cell afferents (Wang and Kaczmarek 1998; Brenowitz and Trussell 2001b; Griesinger et al. 2005; Wang and Manis 2008; Yang and Xu-Friedman 2008). Several studies have suggested

that high levels of presynaptic activity accelerates vesicle replenishment above a baseline recycling rate due to a direct effect of residual calcium levels on the replenishment or endocytosis of vesicles (Dittman and Regehr 1998; Stevens and Wesseling 1998; Wang and Kaczmarek 1998; Xu-Friedman and Regehr 2000; Wu et al. 2009). At NM synapses, recovery from depression has been shown to follow a bi-exponential curve with a fast (tens of ms) and slow (several seconds) component, after both paired-pulse and train stimuli; the fast component was only partly due to postsynaptic desensitization (Brenowitz and Trussell 2001a). In this study we measure and compare the activity-dependence of the recovery from synaptic depression at NA and NM synapses. To determine whether the recovery observed could be explained by a process with multiple kinetic steps, a model based on a sequential, or 'cascading', vesicle pool replenishment was considered. This model had been previously shown to replicate the crossing over of the recovery following high-versus low-rate stimulation that is an indication of activity-dependent recovery, but did not rely on a calcium-feedback mechanism. In this paper we investigated the behavior of the model, and designed a protocol which allowed us to distinguish between the 'cascaded' replenishment model versus a feedback acceleration model.

2 Materials and methods

2.1 Brain slice preparation

All animal procedures were performed in compliance with the guidelines of the Institutional Animal Care and Use Committee of the University of Maryland and the recommendations of the Panel on Euthanasia of the American Veterinary Medical Association. Chicken embryos (E17 ± 1) were rapidly decapitated and quickly submerged in cold, oxygenated (95% O_2–5% CO_2) artificial cerebral spinal fluid (ACSF)(in mM: 130NaCl, 26NaH_2CO_3, 3KCl, 1$CaCl_2$, 2$MgCl_2$, 1.25NaH_2PO_4 3 HEPES, and 10 dextrose). Transverse slices (250 μm) containing NA, NM and afferent auditory nerve fibers were cut using vibrating tissue slicer (Leica Microsystems) in ACSF. Slices were incubated for 30 min at 34°C and then maintained at room temperature (22–24°C). For recordings, slices were continuously perfused with warmed, oxygenated ACSF (30°C, 1–2 ml min^{-1}) that contained 3 mM external calcium, except for data from experiments conducted in a previous study shown in Fig. 1, which used 2 mM external calcium. For all experiments, ACSF contained 20 μM SR955531, 3 μM strychnine, and 50 μM APV (all from Sigma) to isolate AMPA-type excitatory synaptic currents. Cyclothiazide (0.1 mM; Sigma) and aniracetam (2–5 mM; Tocris Cookson) were bath applied; aniracetam recovery controls contained the DMSO vehicle at a concentration of 0.6%. For application of EGTA-AM (EGTA tetra acet-oxymethyl ester; Molecular Probes, a cell-permeant form of EGTA) slices were placed in a secondary incubation at room temperature in ACSF containing EGTA-AM (0.1 mM; 0.6% DMSO vehicle) for 30 min, then washed in normal ACSF for at least 1 h. Controls for EGTA experiments used slices incubated with only the vehicle DMSO.

2.2 Whole-cell recordings

Whole-cell patch-clamp recordings were made from visually identified NA (n = 27) and NM (n = 6) cells using IR/DIC (infrared/differential interference contrast) video microscopy (Stuart et al. 1993). Initial micropipette resistances were 3–7 MΩ with an intracellular voltage-clamp solution of (mM): 70 cesium sulfate, 5 QX-314, 1$MgCl_2$ 1Na_2ATP, 0.3Na_2GTP, 10 phosphocreatine, 4 NaCl, 10 Hepes, 5 BAPTA (1,2-bis(*o*-aminophenoxy)ethane-*N*,*N*,*N*′,*N*′-tetraacetic acid), 32 sucrose and 0.1% biocytin. Electrical recordings were made using an AxoPatch 200B (Axon Instruments, Foster City, CA, USA) in voltage-clamp mode with the series resistance corrected by 60–90% (to a corrected value of 4–8 MΩ). Stimulation and recordings were controlled using custom data acquisition routines written in IGOR Pro (Wavemetrics, Lake Oswego, OR).

2.3 Auditory nerve fiber stimulation

Synaptic currents were evoked with a tungsten monopolar or bipolar electrode placed in the 8th (auditory) nerve fibers tracts as they enter NA at the medial margin and adjusted for amplitude as previously described (MacLeod and Carr 2005). For NM recordings, the stimulation electrode was placed at the dorsal or lateral margin of the nucleus. Fiber paths were often visible under IR-DIC optical conditions. Biphasic stimulus waveforms passed through an analog, constant-current stimulus isolation unit (World Precision Instr., Sarasota, FL). Stimulation artifacts were typically too short to overlap with the EPSCs. Trains of 10 pulses were evoked with a constant stimulus frequency of 50 or 200 Hz, with recovery test pulses delivered at a range of intervals after the last pulse in the train (10 ms to 4 s). Trials were interleaved with intertrial intervals of 12–15 s.

2.4 Analysis

Peak EPSC amplitudes were measured relative to baseline using an exponential fit to account for the decay of the previous EPSC in the train and reported as normalized values relative to the initial EPSC amplitude. Late EPSC ratio, $EPSC_{lt}$, was the ratio of the average of the last 3 EPSCs to the 1st EPSC. Amplitudes of the recovery EPSC, $EPSC_{rec}$, were also normalized to the initial EPSC. All data are reported as mean ± s.d., unless otherwise specified, and statistical testing used Student's *t* test. Exponential fits of the data used the built-in curve-fitting algorithm for a double or single exponential curve in Igor Pro (Wavemetrics, Lake Oswego, OR).

2.5 Model and simulation of short-term synaptic plasticity

The model of short-term synaptic plasticity is based on the concept of neurotransmitter release from a finite release-ready pool of vesicles that must be replenished in a time and concentration gradient dependent manner. Each presynaptic spike releases some fraction,

$F(t)$, of a releasable neurotransmitter vesicle pool, $Q_{ready}(t)$, resulting in a postsynaptic EPSC that is proportional to $F(t)\,Q_{ready}(t)$. The releasable pool, now depleted by $F(t)\,Q_{ready}(t)$, must be replenished from a backup vesicle pool, $Q_{backup}(t)$, which also depletes and then itself needs to be replenished. The vesicle pool state variables Q_{ready} and Q_{backup} represent fractional 'concentrations' that vary from completely 'full' with a value of 1, to completely 'empty' with a value of 0. The recovery of each vesicle pool follows the differential equations in the time interval between action potentials:

$$\frac{dQ_{ready}}{dt} = [\,Q_{backup}(t) - Q_{ready}(t)] \cdot k1 \tag{1}$$

$$\frac{dQ_{backup}}{dt} = [\,1 - Q_{backup}(t)] \cdot k2 - [\,Q_{backup}(t) - Q_{ready}(t) \cdot \frac{k1}{\alpha} \tag{2}$$

where the rate constants $k1$ and $k2$ govern the rates of replenishment and α is the ratio of the maximum sizes of the pools Q_{ready} and Q_{backup} (i.e., $\alpha = Q_{backup\_max}/Q_{ready\_max}$). The sequential refilling of the pools fits an intuitive interpretation of evidence that multiple vesicle cycling pools exist and that replenishment follows a multi-step process (Rizzoli and Betz 2005). The presence of the two rate constants also fit the observation that there must be both slow and fast recovery components (MacLeod et al. 2007).

Facilitation can occur by assuming that each presynaptic spike causes $F(t)$ to increment towards its maximum value of 1:

$$\Delta F\left(t_{\text{spike}}\right) = \left(1 - F\left(t_{\text{spike}}^{-}\right)\right) \cdot \delta_{\text{F}} \tag{3}$$

while decaying between spikes to a baseline value equal to F_0 with the equation:

$$\frac{\mathrm{d}F}{\mathrm{d}t} = -\left(F(t) - F_0\right) \cdot k_{\text{F}} \tag{4}$$

The parameter fitting process used a minimization procedure starting from randomly selected initial parameters. This process measured the difference between model-generated points and experimental data points using an error function:

$$\text{Error} = \sum_{i\,pi=1}^{2} \sum_{n=2}^{20} \left(\frac{\text{EPSC}_{\text{model}}(i\,pi, n) - \text{EPSC}_{\text{data}}(i\,pi, n)}{\sigma_{\text{data}}(i\,pi, n)} \right)^2 \tag{5}$$

with a gradient-descent parameter modification procedure. Many initial conditions were explored to discount local minima solutions. Data points used for fitting the recovery trajectories were ten EPSCs from the stimulus train and the EPSCs measured for ten recovery times for each of two train frequencies (a total of 40 data points). Further model results were produced by using the parameters of these fits and parametrically changing k_{F} (Fig. 6) or α (Fig. 7).

3 Results

3.1 Activity-dependent recovery from depression at cochlear nucleus synapses

Previous experiments were found to suggest that at least part of the rate of recovery of auditory nerve synapses in the avian cochlear nuclei from short-term depression was dependent on the rate of the stimulation of the presynaptic fibers (MacLeod et al. 2007). An example of the activity-dependence of the recovery response following stimulus trains in that study is shown in Fig. 1. To quantitatively characterize the short-term synaptic depression and recovery of auditory nerve synapses, the nerve fibers in brainstem slices were electrically stimulated while recording excitatory postsynaptic currents (EPSCs) from cochlear NA neurons with whole-cell patch-clamp physiology (Fig. 1a). Synaptic responses were evoked using an extracellular electrode placed in the auditory nerve tract and stimulation patterns consisted of pulse trains delivered at a constant frequency, followed by a pulse that is designed to probe recovery and that is presented 2 s after the end of the pulse train. (Fig. 1d).

The recovery of the EPSC after depression was clearly activity-dependent: the EPSCs evoked 2 s after a high-frequency train were larger than EPSCs evoked 2 s after a low-frequency train even though the high-frequency train caused more depression. For a low-frequency stimulus train (10 Hz), the synaptic responses during the train were weakly depressing (Fig. 1b(i)). Increasing the stimulus frequency to 200 Hz resulted in stronger depression during the train (Fig. 1b(ii)). After the 10 Hz train, the EPSC showed very weak recovery to 64% of the initial EPSC amplitude (EPSC_{rec} following the dot-dash lines in Fig. 1b(i), c(i)); after the 200 Hz trains the EPSC showed significantly greater recovery, exceeding that after the 10 Hz train, to 79% of the initial EPSC amplitude ($P < 0.05$; Fig.

1b(ii), c(ii)). The $EPSC_{rec}$ following the 200 Hz train, in fact, was larger (more recovered) than the $EPSC_{rec}$ following the 10 Hz train. We refer to this phenomenon as a 'crossover' effect (Fig. 1c(iii)). The greater recovery observed at that single time point following high-frequency stimulation relative to lower-frequency stimulation is surprising if one assumes that the recovery following both frequency trains occurs with the same time course (e.g., an exponential with a single time constant). Under that assumption, the recovery following the high frequency train should always lag behind the recovery following the lower-frequency train. A crossover in the recovery amplitude indicates that an additional process must contribute to the recovery that depends on the level of activity.

Previous experiments, as illustrated in Fig. 1, probed the recovery following stimulus trains using a single time point at a 2-s delay. In this paper, we report on experiments designed to measure the complete time course of the recovery following trains delivered at two frequencies, 50 or 200 Hz (Fig. 2a). As expected, the 200 Hz stimulus train elicited EPSCs with more than twice the depression than the 50 Hz stimulus train after 10 pulses (Fig. 2b; $EPSC_{lt}$: 200 Hz train, 0.22 ± 0.12; 50 Hz train, 0.50 ± 0.17; $n = 10$). The recovery of the EPSCs following the train, however, was clearly more rapid after the 200 Hz train than after the 50 Hz train. Following 200 Hz stimulation, the recovery trajectory was bi-exponential (τ_{fast} 43.5 ms; τ_{slow} 4.7 s; 62% fast; Fig. 2e). After 50 Hz stimulation, the recovery was complex and non-monotonic, and could not be well fit by a double exponential (Fig. 2c). A single exponential fit could be obtained with the later time points using a time constant of 3.5 s. The recovery trajectories crossed between 50 and 100 ms, after which the 200 Hz recovery trajectory exceeded the 50 Hz recovery trajectory (Fig. 2d; inset, Fig. 2e).

Because the analysis of short-term plasticity at auditory nerve synapses onto NA neurons is complicated by the mixture of short-term synaptic facilitation and depression (MacLeod et al. 2007), we selected our recordings to exclude those that had obvious net facilitation during the trains. We furthermore limited our analysis to those that showed a 'simple' depression profile, defined as a monotonically decreasing EPSC amplitude over the trains, and with at least 30% depression during the final pulses of the 50 Hz stimulus train and greater depression during the 200 Hz stimulus train than during the 50 Hz train. To further minimize any contribution from facilitation we used elevated levels of external calcium to enhance the probability of release (3 mM). Despite these restrictions, a complex recovery curve was observed after 50 Hz stimulation, suggesting an additional dynamic component is part of the recovery process that we were unable to eliminate.

To determine whether this complex recovery was unique to NA, we measured the recovery time course using identical stimulation in NM. The recovery time course measured in NM showed a similar activity-dependence and crossover in the recovery (Fig. 3a), but was always monotonic. Like in NA, the recovery in NM was bi-exponential after 200 Hz (exponential fits shown as solid lines in Fig. 3a; fit for 200 Hz: τ_{fast}, 65.2 ms; τ_{slow}, 3.4 s; 44% fast; $n = 6$). Unlike in NA, the recovery trajectory in NM after 50 Hz was bi-exponential (Fig. 3a; τ_{fast} 46 ms; τ_{slow} 3.2 s; 68% fast). These data suggest that distinct facilitation mechanisms were more prevalent at synapses in NA than in NM, even when the net depression appears similar. Facilitation has been observed at many nerve synapses in NA (MacLeod et al. 2007), but is not typically seen at the endbulb nerve synapses onto neurons in NM even under conditions of reduced probability of release (Brenowitz and Trussell 2001b). In contrast, the crossover in the recovery observed in both NA and NM suggests that activity-dependent recovery is controlled by a common mechanism (or mechanisms) at auditory nerve synapses onto cochlear nucleus neurons.

3.2 Desensitization contributes little to depression at NA synapses

At the developmental age studied here, a portion of the depression at synapses in NM is due to desensitization of the postsynaptic glutamate receptors (Brenowitz and Trussell 2001a). The AMPA-type receptors expressed at synapses in NA have similar properties and are composed of similar subunits as receptors in NM (Raman et al. 1994; Levin et al. 1997; Sugden et al. 2002; MacLeod and Carr 2005). We investigated whether postsynaptic desensitization contributed to short-term depression and recovery of synaptic responses in NA. We measured the short-term depression during 200 Hz trains and the early component of recovery before and after the application of the desensitization blocker aniracetam (2 mM; Fig. 4). Aniracetam significantly prolonged the evoked EPSC, increasing the decay time constant from 1.1 ± 0.2 to 2.3 ± 0.7 ms (single exponential fit; $P < 0.05$, $n = 6$) (Fig. 4b(ii)). Aniracetam also increased the EPSC peak amplitude from control amplitude by ~70% ($P < 0.05$; control $EPSC_1$: 0.70 ± 0.52 nA; aniracetam $EPSC_1$: 1.23 ± 1.13 nA; $n = 5$) (Fig. 4b(i)). Aniracetam slightly relieved the steady state depression during 200 Hz trains in 3 of 5 neurons, but did not have a significant effect on the average degree of depression (control $EPSC_{lt}$: 0.15 ± 0.03; aniracetam $EPSC_{lt}$ = 0.20 ± 0.05; $P = 0.065$; $n = 5$) (Fig. 4b(iii)). Similar results were obtained for depression during 100 Hz trains in 5 mM aniracetam ($EPSC_{lt}$ control: 0.69 ± 0.42; 5 mM aniracetam: 0.75 ± 0.43; $P = 0.27$; $n = 4$) and 100 μM cyclothiazide, another desensitization blocker ($EPSC_{lt}$ control: 0.73 ± 0.48; cyclothiazide: 0.88 ± 0.66; $P = 0.15$; $n = 4$) (data not shown). By contrast, in similar-aged animals, half of the depression seen in synapses in NM during a 200 Hz train is due to postsynaptic receptor desensitization (Brenowitz and Trussell 2001a).

Measurements of the early component of recovery after a 200 Hz train before and after aniracetam (2 mM; Fig. 4c) revealed no change in the recovery time constant (single exponential fit in control: τ_{rec} = 46.9 ms A1: −0.84, y_0 : 0.77; aniracetam: τ_{rec} = 42.1 ms, A1 = −0.78, y_0 = 0.79; $n = 4$). Taken together these results suggest that desensitization shapes the falling phase of the EPSC, but that recovery from desensitization is sufficiently rapid that it makes a negligible contribution to short-term depression.

3.3 Cascade model of replenishment after depletion can reproduce activity-dependent recovery

To test whether the model proposed previously (MacLeod et al. 2007) could account for the activity-dependent recovery, we compared the model with the recovery data. The activity-dependence of the recovery could be explained by several potential mechanisms. Several studies have pointed to a calcium accumulation as a feedback signal that accelerates the vesicle replenishment following depletion (Dittman and Regehr 1998; Stevens and Wesseling 1998; Wang and Kaczmarek 1998). In previous work, we had developed a quantitative model of synaptic release that was able to fit a wide range of synaptic plasticity profiles for responses recorded in NA (MacLeod et al. 2007). The model included vesicle depletion and facilitation, but no activity-dependent feedback. Vesicle replenishment was modeled as a sequential cascade of vesicle cycling with multiple kinetic steps such that vesicles move between distinct pools of different sizes (Fig. 5e). A readily releasable pool released neurotransmitter into the postsynaptic cleft, depleting the pool. A backup pool replenished the ready pool, depleting the backup pool. Two parameters (τ_{ready}, τ_{backup}) controlled the rate of vesicle replenishment of each pool and another parameter modified the relative size of the releasable pool and backup pool. The cascade model could reproduce the crossover in recovery at 2 s fitting simple depression curves using stimulus trains across a wide range of frequencies (10–250 Hz) for both individual recordings (MacLeod et al. 2007) and averaged data (not shown).

To determine whether the same model could fit the full recovery curves, a gradient descent procedure with a cost minimization approach was used to find the six free parameters that provide the best fit of the model to the data. With this procedure, the data could be fit to within an error of less than one standard deviation of the data (Fig. 5a,b; see Sect. 2). The model was able to reproduce both the train responses and the overall trajectory of the recovery, including the bi-exponential recovery and the 'activity-dependent' crossover in the recovery. The best fit of the model (Fig. 5a,b; solid red and blue lines) resulted in a fast replenishment time constant (τ_{ready} = 32 ms) between the backup pool and readily releasable pool and a slow replenishment time constant (τ_{backup} = 4.9 s) from the reserve pool to backup pool. The best fit also occurred when the backup pool was several times larger than the readily releasable pool (α = 5.5). The release probability was 0.47. These vesicle replenishment time constants are very close to both the exponential fits of the recovery in NA (Fig. 2) and to model fits using stimulus trains across a wide range of frequencies (10–250 Hz)(not shown). Holding the replenishment rates fixed to values equal to the exponential fits of the recovery and repeating the fit minimization with four free parameters resulted in a nearly identical fit (Fig. 5a, b, dashed lines).

Since the cascade model as implemented here did not contain any feedback mechanism, the crossover of the recovery must be entirely due to the kinetics of the cascaded vesicle replenishment process. This was an unexpected and counterintuitive result, but can be understood by analyzing the state variables for the vesicle pools. We made two critical assumptions in the model regarding pool sizes and replenishment. First, we assumed that replenishment is driven by the concentration difference between the pools. 'Concentration' is normalized to vary between 1 (full) and 0 (empty). Second, we assumed that the maximal pool sizes may differ (parameter $\alpha \neq 1$) and in our fits the backup pool was several times larger than the readily releasable pool; thus the gain or loss of a vesicle has a greater effect on the concentration of a smaller pool than of the larger pool.

During the stimulus train, vesicles are released from the readily releasable pool, depleting this pool ('Ready pool' curves, Fig. 5c). During the interval between stimuli, the readily releasable pool is replenished with vesicles drawn from the backup pool, depleting the backup pool ('Backup pool', Fig. 5c). Because the interval between pulses is longer during a 50 Hz train (20 ms, blue curves) than during a 200 Hz train (5 ms, red curves), greater recovery of the releasable pool occurs over a single interval, matched by greater depletion of the backup pool. The readily releasable pool becomes depleted rapidly during the 200 Hz train, leading to greater depression of the EPSC; this leads to less cumulative release over the 200 Hz train than over the 50 Hz train (Fig. 5d). The smaller cumulative release means that the backup pool becomes less depleted during the 200 Hz stimulus train than during the 50 Hz stimulus train. When the train ends, the releasable pool quickly replenishes to equalize the readily releasable pool concentration level with the level of the backup pool (right side of Fig. 5c); because the backup pool is less depleted, the recovery curve after the 200 Hz train crosses over the recovery curve for 50 Hz. After equalization between the pools, continued recovery follows the slower exponential recovery of the backup pool as it is itself replenished, producing the bi-exponential recovery trajectory.

3.4 Facilitation at NA synapses influences the recovery curve

In NA recordings, the recovery curve following the 50 Hz train was characterized by a non-monotonic trajectory: there was a prominent 'bump' at the 100 ms time point (Fig. 2c). Notably, the best fit of the model did not reproduce this bump. To determine whether facilitation could underlie the 'bump' in the recovery, we generated recovery curves while modulating the two parameters for facilitation: the facilitation increment parameter, δ_F and τ_F, the facilitation decay time constant. Setting δ_F to 10%, we systematically increased τ_F from 5 to 200 ms. Increasing τ_F increased the amplitude of the EPSCs during the train by up

to ~20% for the 50 Hz train. There was little effect on the EPSC amplitudes during the 200 Hz train (because the increase in release probability was offset by greater depletion) (Fig. 6a,b). When τ_F was 50 ms or longer, the recovery trajectory was non-monotonic, showing a 'bump' at the inflection point between the fast and slow recovery; at 200 ms, the 'bump' was similar in amplitude and duration during the recovery after the 50 Hz train (Fig. 6c). The non-monotonic 'bump', however, was also present after the 200 Hz train, contrary to our data (Fig. 6d). This suggests that facilitation could be responsible for the non-monotonic recovery, but at high frequencies facilitation is limited by some yet unknown factor or ceiling effect.

3.5 Functional effects of the relative sizes of the readily releasable pool and backup pool

Experimental estimates of the sizes of functionally distinct vesicle pools have shown that the number of vesicles available for immediate release is a small fraction of the total recycling pool (Rizzoli and Betz 2004). Our model included a parameter, α, that defined relative sizes of the pools as a ratio. The fitting procedure allowed a wide range of possible pool ratios, from as low as $\alpha = 0.1$ (i.e., the backup pool was ten times smaller than the releasable pool) to $\alpha = 1000$ (i.e., the backup pool was functionally infinite). The best fit of the model to our data produced an intermediate value of α (the backup pool was 5.5 times larger than the releasable pool) that was similar to the range of values found previously for a wide range of synaptic plasticity profiles (α ranged 2–8) (MacLeod et al. 2007). To determine how differences in pool size affect the recovery from depression, model responses were generated while systematically varying α. If α was low (e.g., $\alpha = 1$), the EPSC amplitudes during the slower train did not reach steady state (Fig. 7a) and recovery was slow, limited by the rate of recovery of the backup pool (Fig. 7c, top left graph). If α was high, the model reduced to approximate a single-step replenishment model, which reached a steady state (e.g., Fig. 7a), but was dominated by a single time constant (τ_{ready}), which failed to fit the bi-exponential recovery and eliminated the crossover (Fig. 7c, bottom right graph). No crossover effect was ever observed for any combination of parameters when we explicitly modeled a single-step replenishment model. The serial replenishment between the two pools was therefore an essential feature for generating the activity-dependent differences in the recovery curves.

3.6 Testing the model

A leading hypothesis for the activity-dependent fast recovery and crossover proposes that calcium accumulation during high-frequency activity accelerates vesicle replenishment (Dittman and Regehr 1998; Wang and Kaczmarek 1998; Dittman et al. 2000). Because the cascaded pool model proposed here and the calcium-dependent model both produce the same crossover effect following simple trains, we used combination trains that delivered the same interspike intervals, but in a pattern that allowed us to distinguish between the predictions of the two models. These two patterns consisted of either 15 pulses delivered at intervals of 200 ms (a 5 Hz rate) and followed by 14 pulses delivered at intervals of 10 ms (a 100 Hz rate), or the 29 pulses presented in the opposite order. In all cases, a "recovery pulse" was presented 1 s after the end of the train (Fig. 8a). The cascade model clearly predicts that no crossover should occur during the recovery period (Fig. 8b). This model behavior is due to a depletion of the backup pool during the early low-frequency trains in the 5 Hz/100 Hz trains, which suppresses the degree of rapid recovery at the end of the train. During the 100 Hz/5 Hz train, the readily releasable pool is quickly depleted, limiting cumulative release during the trains reducing its drain on the backup pool, and allowing quicker recovery at the end of the train. In contrast, if calcium accumulation during high frequency stimulation is driving the rapid recovery, we hypothesize that following a low-frequency train with a high frequency (5 Hz before 100 Hz), should accelerate recovery; conversely, following a high frequency train with a sufficiently long low-frequency train

should allow the calcium accumulation to diminish and preventing acceleration of recovery following the train. By this reasoning, if the calcium-dependent mechanism underlies the recovery, crossover should still occur with the mixed frequency trains. When tested with the combination trains, the experimental data showed responses during the trains that closely matched the cascade model output (Fig. 8c, during pulses 1–29). However, the model prediction and data were distinctly different when the recovery EPSC was measured. The $EPSC_{rec}$ amplitude at a delay of 1 s was greater when immediately preceded by 100 Hz stimulation (red symbol) than 5 Hz (blue symbol; Fig. 8c; $n = 8$), contrary to the prediction of the cascade model (arrow in Fig. 8b, recovery panel).

4 Discussion

Auditory nerve fibers fire action potentials at very high rates during spontaneous and sensory driven activity, often at sustained rates of 300 Hz or more. The synapses between the nerve fibers and their targets therefore must have mechanisms to cope with high levels of exocytosis. Rapid forms of synaptic recovery (i.e., with time constants shorter than 100 ms) have been described at several specialized synapses of the auditory system: at hair cell synapses onto auditory nerve afferents (Griesinger et al. 2005), the calyx of Held synapses onto neurons of the medial nucleus of the trapezoid body (MNTB) (Wang and Kaczmarek 1998; Sakaba and Neher 2001), the endbulb synapses onto the bushy cells of the anterior ventral cochlear nucleus (AVCN) (Wang and Manis 2008; Yang and Xu-Friedman 2008), and the endbulb synapses onto the avian NM neurons (Brenowitz and Trussell 2001a). Our experiments demonstrate an equally rapid recovery from short-term synaptic depression at the auditory nerve synapses that transmit sound intensity information to the neurons of the avian cochlear nucleus angularis, which use less specialized, non-endbulb terminals. These results suggest that rapid recovery is a feature of synapses in all neural pathways that must cope with high firing rates. Short breaks in presynaptic activity would be sufficient to allow these auditory synapses to recover the majority (up to 80%) of their synaptic strength. Because many auditory stimuli such as speech phonemes or birdsong syllables occur in short bursts separated by gaps of relative quiet (Brenowitz et al. 1997; Doupe and Kuhl 1999), rapid synaptic recovery may allow the auditory system to respond efficiently to natural stimuli despite high transient firing rates or even serve as a mechanism to perform gap detection.

4.1 Mechanisms of depression in the intensity pathway

Our results show that, at NA synapses, postsynaptic receptor desensitization contributed only marginally to short-term depression during the trains and negligibly to the rapid recovery from depression. In contrast, desensitization appears to play a role in determining the duration of the EPSCs. Like other auditory brainstem neurons, NA synapses typically express AMPA-type glutamatergic neurotransmitter receptors that are composed of subunits that confer rapid kinetics and calcium-permeability, as well as desensitization in the continued presence of neurotransmitter (Raman et al. 1994; Levin et al. 1997; Sugden et al. 2002; MacLeod and Carr 2005). However, the lack of desensitization observed here under synaptic stimulation was not too surprising, given that the release probability is likely to be much lower, and release occurs at small (compared to NM) bouton-like terminals (Carr and Boudreau 1991). Endbulb synapses, like those in NM, release large amounts of neurotransmitter during evoked responses into the cleft. In relatively young animals such as used in our study, the resulting postsynaptic receptor desensitization can significantly contribute to short-term synaptic depression and a rapid recovery from this desensitization contributes to some, but not all, of the rapid recovery from depression (Otis et al. 1996; Brenowitz and Trussell 2001a; Wong et al. 2003; Yang and Xu-Friedman 2008). The smaller size of the conventional terminals in NA (Carr and Boudreau 1991) and a lower

release probability likely limit accumulation of neurotransmitter in the cleft and the degree of desensitization. Desensitization, however, appears to be greatly reduced in mature animals (Wang and Manis 2008, Renden et al. 2005; Brenowitz and Trussell 2001a) and therefore may not be a major distinguishing factor between NA and NM synapses at maturity.

4.2 Facilitation and rapid recovery may overlap

Short-term facilitation and its effect on the synaptic filtering properties appears to be an important distinction between the synapses in the intensity pathway and the timing pathway. In this study, we found that the fast and slow time constants of recovery after high frequency trains were markedly similar at synapses in both NA and NM, and in both cases recovery showed activity-dependence. The primary difference was seen in the uneven, non-monotonic recovery trajectory following low-frequency stimulus at synapses in NA, but not in NM. The most likely explanation for this difference is an overlapping decay of short-term facilitation with the recovery from depression. Net facilitation of synaptic responses was commonly observed at synapses in NA under lower external calcium concentrations than used here (MacLeod et al. 2007), and, less frequently, during this study with 3 mM calcium (data not shown). The synapses analyzed in this paper were selected on the basis of their depression profile in order to study the recovery from depression. Despite this, the NA synapses were clearly less depressing than the NM synapses, and we cannot exclude that some facilitation may contribute to the responses. Our model results showed that the inclusion of short-term facilitation (implemented as an activity-dependent increase in the probability of release) reduced the depression during the 50 Hz train, and produced in a ‘bump’ in the recovery curve, suggesting that the competing effects of the decay of facilitation and recovery from vesicle depletion could account for the non-monotonic recovery. The model and data did not comport, however, over the recovery trajectory following the high frequency train: the model shows a clear bump in the trajectory while the data do not. The facilitation as implemented in this study was highly simplified, however, and modification of the model is clearly needed to explain this discrepancy. Further work is necessary to determine whether differences in the expression of facilitation between the cochlear nuclei might arise due to simple differences in the probability of release, or the presence of distinct facilitation mechanisms at the nerve terminals.

4.3 Activity-dependent recovery from short-term depression is a common feature in the cochlear nucleus

In both NA and NM, the recovery after short-term depression was dependent on the presynaptic stimulation frequency, so much so that the high frequency stimulation resulted greater recovery after a 2-s delay than the lower-frequency stimulation, seen as a clear crossover in the recovery trajectories. While a number of mechanisms could contribute to the short-term depression and recovery, including postsynaptic desensitization in the case of NM, a large component is likely to be due to the depletion of release-ready synaptic vesicles. If so, the fast and slow components of the recovery could be due to a rapid recruitment of vesicles to the active zone, followed by slower recruitment to return to baseline levels. Such behavior could be explained several ways, such as the presence of multiple kinetic steps during recruitment, multiple parallel vesicle pools with different recovery kinetics (Sakaba and Neher 2001; Hosoi et al. 2007), or activity-dependent acceleration of vesicle recruitment (Dittman and Regehr 1998; Stevens and Wesseling 1998; Wang and Kaczmarek 1998; Xu-Friedman and Regehr 2000; Wu et al. 2009). Other potential contributors that were not investigated include a direct refractoriness of release due to presynaptic mechanisms such as calcium channel inactivation, or other neuromodulatory feedback mechanisms.

In this study, we explored the potential for the hypothesis of multiple kinetic steps during recruitment to account for the recovery from depression, in part because this hypothesis has received less attention than in previous studies. Indeed, given the experimental evidence for multiple vesicle pools, variously defined, it would seem important to understand how the dynamics of pool replenishment during activity affects synaptic release and short-term plasticity. Surprisingly, we found that a quantitative model of synaptic transmission originally designed for an earlier study (MacLeod et al. 2007) could, without modification, reproduce the phenomenon of activity-dependent recovery. The model was considered because it succinctly explained both the rapid component of the recovery time course and the activity-dependence, and was based on a plausible scenario of sequential vesicle pool replenishment with multiple kinetic steps. In the model presented here the rapid recovery is due the presence of a fast time constant (~40 ms) of replenishment of the readily releasable vesicle pool. The activity-dependence arose due to the frequency-dependence of the depletion of the backup pool, which was the results of two key features. (1) Both pools had a finite maximal size (defined by the size at rest) and were depleted during activity. The maximal size of the backup pool was larger than that of the releasable pool. (2) Vesicle movement was driven by a ‘concentration’ difference between the pools. The apparent activity-dependence was a direct result of difference in the cumulative depletion of the backup pool and the kinetics of the sequential replenishment. Using stimulation trains composed of sequences of different frequencies, however, our data showed that the multiple kinetic step hypothesis alone cannot account for the recovery: the model predicted a lack of crossover in the recovery, while the data showed a clear crossover. This suggests that another activity-dependent mechanism is present, such as a calcium-dependent acceleration of the recovery.

Recovery from short-term depression has been shown to be sensitive to presynaptic calcium levels in a number of previous studies. Fast recovery from depression was slowed by manipulations of calcium such as reduced extracellular calcium (Dittman and Regehr 1998; Wang and Manis 2008), or loading the presynaptic terminals with EGTA (Dittman and Regehr 1998; Yang and Xu-Friedman 2008) or calmodulin inhibitors (Sakaba and Neher 2001; Hosoi et al. 2007; Wang and Manis 2008). Under a calcium-feedback hypothesis, models of activity-dependent recovery could reproduce the recovery by assuming the replenishment of the readily releasable vesicle pool occurs with a slow baseline rate during low activity levels, but during high activity levels, residual calcium accumulation accelerates the replenishment rate, implemented computationally by making the single replenishment rate activity- and time-dependent (Dittman et al. 2000; Fuhrmann et al. 2002; Hosoi et al. 2007). On the other hand, the fast phase of recovery persisted at the endbulb synapses in NM under reduced calcium conditions (1.5 mM external calcium) (Brenowitz and Trussell 2001a); similar results have recently been described in MNTB (Lorteije et al. 2009). In our own test of the contribution of residual calcium at synapses in NA, presynaptic terminals were loaded with EGTA by incubating slices with a cell-permeant form and the recovery of the EPSC from depression tested. This manipulation slowed the early component of the recovery compared to sham incubated controls, but failed to eliminate the crossover in the recovery trajectory (Supplementary Fig. S1; see Sect. 2). These results suggest less sensitivity to residual calcium level changes due to activity than other studies have found, but further testing remains to be done. Manipulation of residual or basal calcium levels with a chelator like EGTA is an imperfect test, however, as it is likely to affect multiple presynaptic elements, including endocytosis and replenishment (Wu et al. 2009), facilitation (Zucker 1999) and possibly other components of the recycling process or baseline pool size. Many interrelated factors may directly or indirectly affect the kinetics of release and ultimately short-term plasticity. The results presented here, along with other published models using a calcium-dependent recovery, suggest that different models can reproduce

similar effects, and explicit modeling leads to testable predictions that might otherwise be difficult to intuit.

While the concept of vesicle cycling as a complex process is well accepted, the consequences of sequential pool replenishment on the dynamics of transmitter release and the resulting short-term plasticity are poorly understood. Studies have repeatedly shown that models of short-term depression using a simple first order process do not adequately capture the dynamics of synaptic strength. Incorporating additional vesicle pools to release-ready pools in a cascaded (sequential) process (Saviane and Silver 2006) adds a level of complexity that may be a reflection of the biophysical process. The journey of a synaptic vesicle to its destination in the active zone and its eventual release involves multiple steps, including endocytosis, refilling, docking, and priming (Sudhof 2004). The cascaded vesicle replenishment model is consistent with evidence indicating the presence multiple subsets of vesicles: numerous studies describe a pool of immediately releasable vesicles, a recycling vesicle pool, and a reserve pool, although these are operational definitions that depend on the specific methodology and can be difficult to compare across model systems (Schneggenburger et al. 2002; Rizzoli and Betz 2004). In our implementation of the cascade model, we define a readily releasable pool whose vesicles can be triggered to undergo exocytosis by single action potentials, and thus would correspond to docked, primed vesicles close to the calcium influx site. Our backup pool feeds the releasable pool with a rapid time course; the backup pool and the readily releasable pool together would correspond to the more common definition of the recycling pool. This time course could correspond to translocation of more distant, but primed, vesicles to be closer to the calcium trigger (Wadel et al. 2007) or a final step readying docked and primed vesicles for release (Chang and Sudhof 2009). One simplifying assumption is that the backup pool itself is continuously replenished. The source of these vesicles could be due to continuous endocytosis and/or recruitment from a ‘reserve’ pool; our time constant for backup pool replenishment is consistent with fast endocytosis (Wu et al. 2007). The ratio of the backup versus releasable pool sizes estimated in our model (a factor between two and ten) is similar to estimates of the ratio of releasable vesicles to total recycling vesicles (Schneggenburger et al. 2002; Rizzoli and Betz 2004). We neither constrain the total size of the recycling pool nor consider it a closed system; it is unclear at this time how and under what conditions the recycling pool and a ‘reserve’ pool intermingle. Explicit quantitative models are critical for hypothesis testing and, as we show, subtle changes in the assumptions for even a simple model can produce unexpected results.

4.4 Physiological effects of short-term synaptic plasticity in vivo

The evidence supporting the functional significance of short-term synaptic plasticity as a mechanism that contributes to neural coding is heavily dependent on in vitro slice physiology and computational studies. Although it is critically important to test these effects in the intact brain, there are only a few studies to date that directly and adequately assess synaptic plasticity in vivo, and among those studies, results have been mixed. Good evidence for the functional importance of short-term plasticity exists in the electric fish electrosensory system, where synaptic depression contributes to the coding of directional selectivity (Fortune and Rose 2000, 2002; Carver et al. 2008). In vitro studies show that short-term depression dominates at thalamocor-tical synapses (Abbott and Regehr 2004). In vivo, short-term depression was confirmed in barrel cortex (Chung et al. 2002), but in visual cortex, where the short-term depression was hypothesized to relate to directional selectivity and/or sensory adaptation (Chance et al. 1998; Carandini et al. 2002), in vivo studies have been contradictory, finding little modification of synaptic strength (Boudreau and Ferster 2005) or facilitation (Usrey et al. 2000). In the auditory brainstem pathways, the profound short-term depression observed in vitro has not been confirmed in vivo (Young and Sachs

2008; Lorteije et al. 2009). This finding may be due to the likelihood that depression is less pronounced in older animals, which, combined with suprathreshold amplitude of the synaptic potential, suggests that even moderate depression may have little practical effect. One could argue, however, that there appears to be little computational value for short-term plasticity to modulate neural activity at these synapses which are otherwise tuned to be reliable, precisely timed relays. The pronounced depression profiles in vitro may be a byproduct of their high reliability. Instead, one should investigate short-term plasticity at smaller synapses that are more representative of a typical synapses, where modulation of synaptic strength would have a predictable effect on the integration of inputs. Further work to understand the role of plasticity in the intensity circuits and how they could contribute to interaural level difference coding, amplitude modulation coding, or sound recognition would provide an important next step in understanding the functional role of short-term plasticity in sensory processing.

Supplementary Material

Refer to Web version on PubMed Central for supplementary material.

Acknowledgments

The authors thank C.E. Carr for helpful discussions on earlier versions of the manuscript. This work was supported by a grant from the National Institute on Deafness and other Communication Disorders (NIDCD/NIH) DC007972 to KMM, and Air Force Office of Scientific Research Grant FA95500410130 and National Science Foundation Grant CCF0347573 to TKH.

References

Abbott LF, Regehr WG. Synaptic computation. Nature. 2004; 431:796–803. [PubMed: 15483601]

Blitz DM, Foster KA, Regehr WG. Short-term synaptic plasticity: a comparison of two synapses. Nat Rev Neurosci. 2004; 5:630–640. [PubMed: 15263893]

Boudreau CE, Ferster D. Short-term depression in thalamocortical synapses of cat primary visual cortex. J Neurosci. 2005; 25:7179–7190. [PubMed: 16079400]

Brenowitz S, Trussell LO. Maturation of synaptic transmission at end-bulb synapses of the cochlear nucleus. J Neurosci. 2001a; 21:9487–9498. [PubMed: 11717383]

Brenowitz S, Trussell LO. Minimizing synaptic depression by control of release probability. J Neurosci. 2001b; 21:1857–1867. [PubMed: 11245670]

Brenowitz EA, Margoliash D, Nordeen KW. An introduction to birdsong and the avian song system. J Neurobiol. 1997; 33:495–500. [PubMed: 9369455]

Cao XJ, McGinley MJ, Oertel D. Connections and synaptic function in the posteroventral cochlear nucleus of deaf jerker mice. J Comp Neurol. 2008; 510:297–308. [PubMed: 18634002]

Carandini M, Heeger DJ, Senn W. A synaptic explanation of suppression in visual cortex. J Neurosci. 2002; 22:10053–10065. [PubMed: 12427863]

Carr CE, Boudreau RE. Central projections of auditory nerve fibers in the barn owl. J Comp Neurol. 1991; 314:306–318. [PubMed: 1723997]

Carver S, Roth E, Cowan NJ, Fortune ES. Synaptic plasticity can produce and enhance direction selectivity. PLoS Comput Biol. 2008; 4:e32. [PubMed: 18282087]

Chance FS, Nelson SB, Abbott LF. Synaptic depression and the temporal response characteristics of V1 cells. J Neurosci. 1998; 18:4785–4799. [PubMed: 9614252]

Chang WP, Sudhof TC. SV2 renders primed synaptic vesicles competent for Ca^{2+}-induced exocytosis. J Neurosci. 2009; 29:883–897. [PubMed: 19176798]

Chung S, Li X, Nelson SB. Short-term depression at thalamocortical synapses contribute to rapid adaptation of cortical sensory responses in vivo. Neuron. 2002; 34:437–446. [PubMed: 11988174]

Cook DL, Schwindt PC, Grande LA, Spain WJ. Synaptic depression in the localization of sound. Nature. 2003; 421:66–70. [PubMed: 12511955]

Dittman JS, Regehr WG. Calcium dependence and recovery kinetics of presynaptic depression at the climbing fiber to Purkinje cell synapse. J Neurosci. 1998; 18:6147–6162. [PubMed: 9698309]

Dittman JS, Kreitzer AC, Regehr WG. Interplay between facilitation, depression, and residual calcium at three presynaptic terminals. J Neurosci. 2000; 20:1374–1385. [PubMed: 10662828]

Doupe AJ, Kuhl PK. Birdsong and human speech: common themes and mechanisms. Annu Rev Neurosci. 1999; 22:567–631. [PubMed: 10202549]

Fortune ES, Rose GJ. Short-term synaptic plasticity contributes to the temporal filtering of electrosensory information. J Neurosci. 2000; 20:7122–7130. [PubMed: 10995860]

Fortune ES, Rose GJ. Roles for short-term synaptic plasticity in behavior. J Physiol Paris. 2002; 96:539–545. [PubMed: 14692501]

Fuhrmann G, Segev I, Markram H, Tsodyks M. Coding of temporal information by activity-dependent synapses. J Neurophysiol. 2002; 87:140–148. [PubMed: 11784736]

Griesinger CB, Richards CD, Ashmore JF. Fast vesicle replenishment allows indefatigable signalling at the first auditory synapse. Nature. 2005; 435:212–215. [PubMed: 15829919]

Hosoi N, Sakaba T, Neher E. Quantitative analysis of calcium-dependent vesicle recruitment and its functional role at the calyx of Held synapse. J Neurosci. 2007; 27:14286–14298. [PubMed: 18160636]

Kuba H, Koyano K, Ohmori H. Synaptic depression improves coincidence detection in the nucleus laminaris in brainstem slices of the chick embryo. Eur J Neurosci. 2002; 15:984–990. [PubMed: 11918658]

Levin MD, Kubke MF, Schneider M, Wenthold R, Carr CE. Localization of AMPA-selective glutamate receptors in the auditory brainstem of the barn owl. J Comp Neurol. 1997; 378:239–253. [PubMed: 9120063]

Lorteije JA, Rusu SI, Kushmerick C, Borst JG. Reliability and precision of the mouse calyx of Held synapse. J Neurosci. 2009; 29:13770–13784. [PubMed: 19889989]

MacLeod KM, Carr CE. Synaptic physiology in the cochlear nucleus angularis of the chick. J Neurophysiol. 2005; 93:2520–2529. [PubMed: 15615833]

MacLeod KM, Carr CE. Beyond timing in the auditory brainstem: intensity coding in the avian cochlear nucleus angularis. Prog Brain Res. 2007; 165:123–133. [PubMed: 17925243]

MacLeod KM, Horiuchi TK, Carr CE. A role for short-term synaptic facilitation and depression in the processing of intensity information in the auditory brain stem. J Neurophysiol. 2007; 97:2863–2874. [PubMed: 17251365]

Markram H, Gupta A, Uziel A, Wang Y, Tsodyks M. Information processing with frequency-dependent synaptic connections. Neurobiol Learn Mem. 1998; 70:101–112. [PubMed: 9753590]

O'Donovan MJ, Rinzel J. Synaptic depression: a dynamic regulator of synaptic communication with varied functional roles. Trends Neurosci. 1997; 20:431–433. [PubMed: 9347607]

Oertel D. The role of timing in the brain stem auditory nuclei of vertebrates. Annu Rev Physiol. 1999; 61:497–519. [PubMed: 10099699]

Otis TS, Wu YC, Trussell LO. Delayed clearance of transmitter and the role of glutamate transporters at synapses with multiple release sites. J Neurosci. 1996; 16:1634–1644. [PubMed: 8774432]

Raman IM, Zhang S, Trussell LO. Pathway-specific variants of AMPA receptors and their contribution to neuronal signaling. J Neurosci. 1994; 14:4998–5010. [PubMed: 7913958]

Renden R, Taschenberger H, Puente N, Rusakov DA, Duvoisin R, Wang LY, Lehre KP, von Gersdorff H. Glutamate transporter studies reveal the pruning of metabotropic glutamate receptors and absence of AMPA receptor desensitization at mature calyx of Held synapses. J Neurosci. 2005; 25:8482–8497. [PubMed: 16162930]

Rizzoli SO, Betz WJ. The structural organization of the readily releasable pool of synaptic vesicles. Science. 2004; 303:2037–2039. [PubMed: 15044806]

Rizzoli SO, Betz WJ. Synaptic vesicle pools. Nat Rev Neurosci. 2005; 6:57–69. [PubMed: 15611727]

Sakaba T, Neher E. Calmodulin mediates rapid recruitment of fast-releasing synaptic vesicles at a calyx-type synapse. Neuron. 2001; 32:1119–1131. [PubMed: 11754842]

Saviane C, Silver RA. Fast vesicle reloading and a large pool sustain high bandwidth transmission at a central synapse. Nature. 2006; 439:983–987. [PubMed: 16496000]

Schneggenburger R, Sakaba T, Neher E. Vesicle pools and short-term synaptic depression: lessons from a large synapse. Trends Neurosci. 2002; 25:206–212. [PubMed: 11998689]

Stevens CF, Wesseling JF. Activity-dependent modulation of the rate at which synaptic vesicles become available to undergo exocytosis. Neuron. 1998; 21:415–424. [PubMed: 9728922]

Stuart GJ, Doft HU, Sakmann B. Patch-clamp recordings from the soma and dendrites of neurons in brain slices using infrared video microscopy. Pflugers Arch. 1993; 423:511–518. [PubMed: 8351200]

Sudhof TC. The synaptic vesicle cycle. Annu Rev Neurosci. 2004; 27:509–547. [PubMed: 15217342]

Sugden SG, Zirpel L, Dietrich CJ, Parks TN. Development of the specialized AMPA receptors of auditory neurons. J Neurobiol. 2002; 52:189–202. [PubMed: 12210103]

Trussell LO. Synaptic mechanisms for coding timing in auditory neurons. Annu Rev Physiol. 1999; 61:477–496. [PubMed: 10099698]

Trussell LO. Modulation of transmitter release at giant synapses of the auditory system. Curr Opin Neurobiol. 2002; 12:400–404. [PubMed: 12139987]

Usrey WM, Alonso JM, Reid RC. Synaptic interactions between thalamic inputs to simple cells in cat visual cortex. J Neurosci. 2000; 20:5461–5467. [PubMed: 10884329]

von Gersdorff H, Borst JG. Short-term plasticity at the calyx of held. Nat Rev Neurosci. 2002; 3:53–64. [PubMed: 11823805]

Wadel K, Neher E, Sakaba T. The coupling between synaptic vesicles and Ca^{2+} channels determines fast neurotransmitter release. Neuron. 2007; 53:563–575. [PubMed: 17296557]

Wang L-Y, Kaczmarek LK. High-frequency firing helps replenish the readily releasable pool of synaptic vesicles. Nature. 1998; 394:384–388. [PubMed: 9690475]

Wang Y, Manis PB. Short-term synaptic depression and recovery at the mature mammalian endbulb of Held synapse in mice. J Neurophysiol. 2008; 100:1255–1264. [PubMed: 18632895]

Wong AY, Graham BP, Billups B, Forsythe ID. Distinguishing between presynaptic and postsynaptic mechanisms of short-term depression during action potential trains. J Neurosci. 2003; 23:4868–4877. [PubMed: 12832509]

Wu LG, Ryan TA, Lagnado L. Modes of vesicle retrieval at ribbon synapses, calyx-type synapses, and small central synapses. J Neurosci. 2007; 27:11793–11802. [PubMed: 17978015]

Wu XS, McNeil BD, Xu J, Fan J, Xue L, Melicoff E, Adachi R, Bai L, Wu LG. Ca(2+) and calmodulin initiate all forms of endocytosis during depolarization at a nerve terminal. Nat Neurosci. 2009; 12:1003–1010. [PubMed: 19633667]

Xu-Friedman MA, Regehr WG. Probing fundamental aspects of synaptic transmission with strontium. J Neurosci. 2000; 20:4414–4422. [PubMed: 10844010]

Yang H, Xu-Friedman MA. Relative roles of different mechanisms of depression at the mouse endbulb of Held. J Neurophysiol. 2008; 99:2510–2521. [PubMed: 18367696]

Young ED, Sachs MB. Auditory nerve inputs to cochlear nucleus neurons studied with cross-correlation. Neuroscience. 2008; 154:127–138. [PubMed: 18343587]

Zucker RS. Calcium- and activity-dependent synaptic plasticity. Curr Opin Neurobiol. 1999; 9:305–313. [PubMed: 10395573]

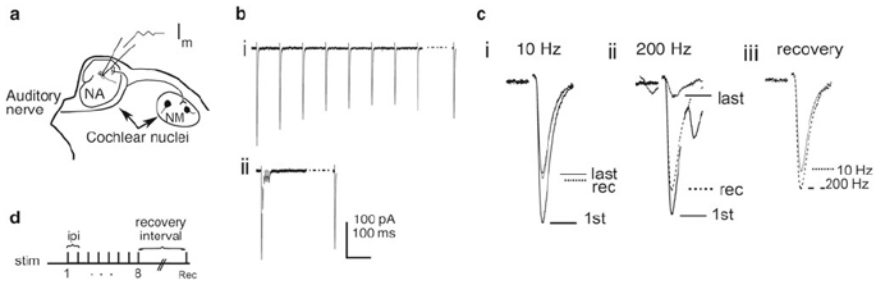

Fig. 1.

Recovery from short-term synaptic depression in the cochlear nucleus angularis is activity-dependent **a** Cross-section schematic of chick auditory brainstem and the cochlear nuclei: *NA* nucleus angularis, *NM* nucleus magnocellularis, I_m membrane current recorded under voltage clamp. Recordings were also performed in NM. Auditory nerve fibers bifurcate to send one branch each to NA and NM. **b** Excitatory postsynaptic currents recorded in an NA neuron in response to auditory nerve stimulation followed by a single recovery test stimulus pulse. (*i*) 10Hz stimulus train, (*ii*) 200Hz stimulus train. **c** Overlay of initial EPSC, last EPSC in the train, and recovery EPSC. (*i*) EPSCs with 10Hz stimulation and (*ii*) 200Hz stimulation. (*iii*) Overlay of the recovery EPSCs for 10 and 200Hz trains. **d** Stimulus trains for these experiments consisted of 8 pulses at a constant frequency followed by a 2-s recovery interval

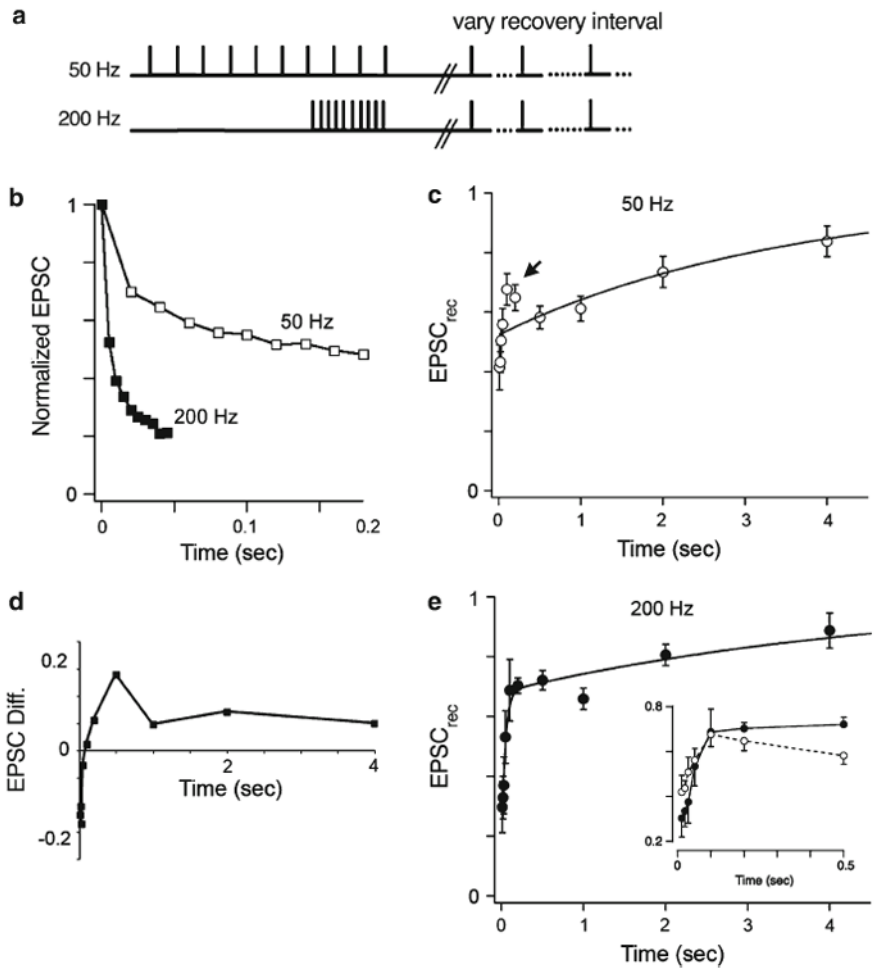

Fig. 2.

Time course of activity-dependent recovery from depression in nucleus angularis. **a** Stimuli consisted of 50 and 200 Hz trains, followed by recovery test stimuli at varying intervals from 10ms to 4s. **b** Average train responses for NA neurons (n = 10). **c,e** Recovery of EPSC amplitudes (markers; n = 10) after the 50 Hz train (**c**) and 200 Hz train (**e**). Amplitudes are normalized to the initial EPSC amplitude. Exponential fits of the data are shown as *solid lines*: single exponential in **c** and double exponential in **e**. *Inset* in **e**: overlay of data for 50 and 200Hz during early recovery shows crossover. Data are mean ± s.e.m. **d** Difference between the two recovery trajectories [$EPSC_{rec}$ (200 Hz) – $EPSC_{rec}$ (50 Hz)]. Positive values indicate when the 200 Hz recovery EPSCs exceeded 50 Hz recovery EPSCs

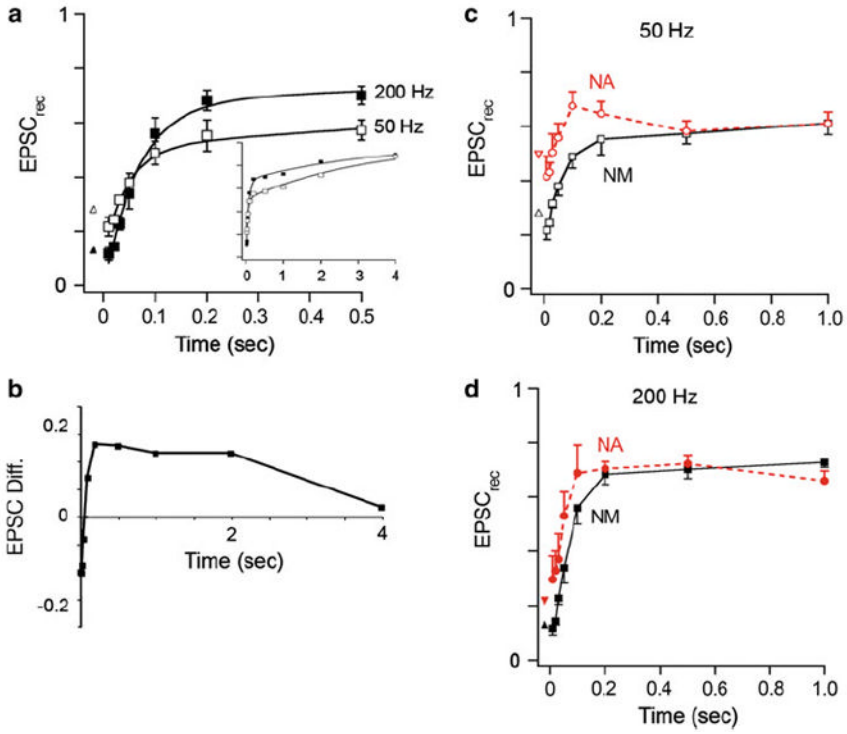

Fig. 3.

Activity-dependent recovery from depression in nucleus magnocellularis. **a** Recovery of EPSC amplitudes for ANF synapses in NM was also activity-dependent (n = 6). Markers, recovery EPSC amplitudes; *solid lines*, exponential fits of the data. *Triangle symbols* indicated the steady state depression level during 50 Hz train (*open triangle*) or 200 Hz train (*closed triangle*) preceding recovery. *Inset* recovery trajectories over full 4 s recovery interval, *same symbols*. Data are mean ± s.e.m. **b** Difference between 200 and 50 Hz train recovery EPSCs in **a. c** Overlay of the early part of the recovery data for NA and NM following the 50 Hz train showed that NM recovery was monotonic, without the 'bump' seen in the NA recovery. *Triangle symbols* as in **a**, except *inverted triangle* indicates the NA steady state depression level preceding recovery. **d** Overlay of the early part of the recovery data for NA and NM following the 200 Hz train showed similar fast and slow components. *Triangle symbols* as in **a**, except *inverted triangle* indicates the NA steady state depression level preceding recovery

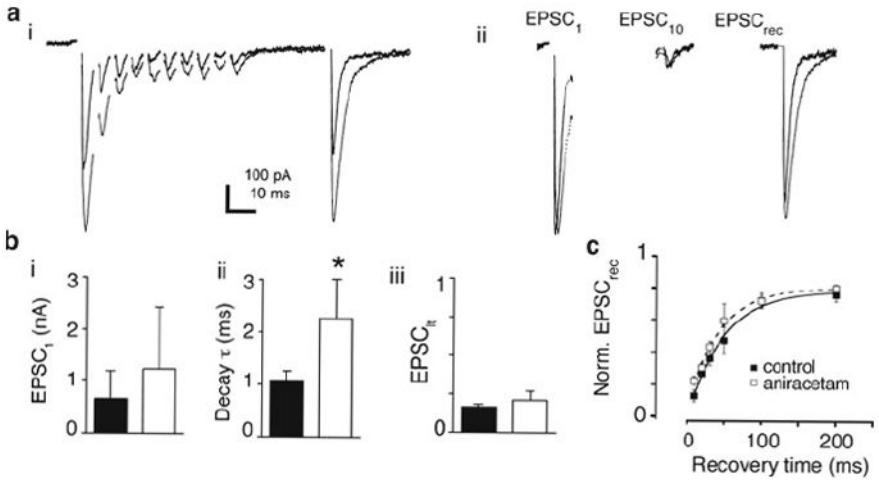

Fig. 4.

Desensitization contributes little to short-term depression in NA. **a** EPSCs during 200 Hz train and recovery (30ms recovery interval) in control (*bold line*) and in aniracetam (*thin line*). Comparison of unscaled traces (*i*) and traces scaled by their initial EPSC amplitudes (*ii*) show that the EPSC amplitudes are increased and time courses are prolonged, but there was no relief of depression by aniracetam ($EPSC_{10}$ and $EPSC_{rec}$ are similar in (*ii*)) in this recording. **b** Summary data for initial EPSC amplitude (*i*), EPSC decay time constant (*ii*) and steady state depression of the train (*iii*). **c** Early time course of the recovery is unchanged in aniracetam. Exponential fits for control (*solid line*) and aniracetam (*dashed line*) data have indistinguishable time constants ($\tau_{control}$ = 46.9ms; $\tau_{aniracetam}$ = 42.1ms). Data are mean ± s.e.m.

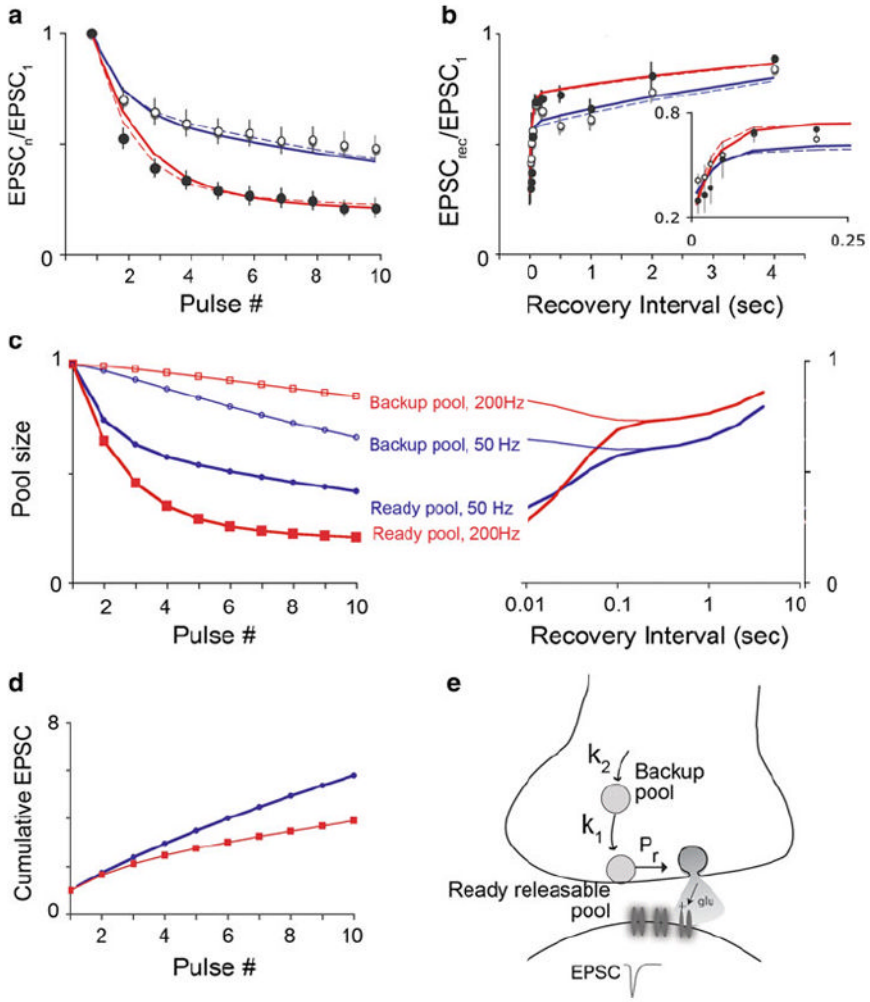

Fig. 5.

The best fit of the cascade model closely approximated the data for simple trains. *Lines* show the model fit during the trains (**a**) and during the recovery curves (**b**). Markers replot the data from Fig. 3: *open markers*, 50 Hz data; *closed markers*, 200 Hz data. Model fits that were found using a gradient descent algorithm with all parameters free are represented by the *solid lines: blue* 50Hz model EPSC estimates, *red* 200Hz model EPSC estimates. The *dashed lines* represent an alternative fitting where *k*1 and *k*2 in the modelwere fixed to the inverse of τ_{fast} and τ_{slow}, respectively, from the exponential fit of the 200 Hz recovery data in Fig. 2d. **c** Evolution of the pool state variable during trains and recovery. *Left* Pool sizes during the trains showing the depletion of the ready-releasable pool ("Ready pool"; *solid markers*, *thick line*) and the backup pool (*open markers*, *thin line*). For clarity, only the values at the times of the stimulus are plotted. *Right* Time-dependent recovery of both pools with clear crossover of the ready pools. The continuous value of the state variable versus time is plotted as a log scale. The recovery EPSC amplitudes (plotted in **b**) is directly proportional to the ready pool concentration. **d** Cumulative EPSC over the course of the trains showed greater neurotransmitter release, in total, during 50 Hz activity (*blue*) than during 200 Hz activity (*red*). **e** Schematic of the cascade model. See text. *k*1 and *k*2 are rate constants of the cascaded (sequential) vesicle replenishment process, while Pr is the fraction of the readily releasable pool vesicles that undergo exocytosis at the time of the presynaptic action potential

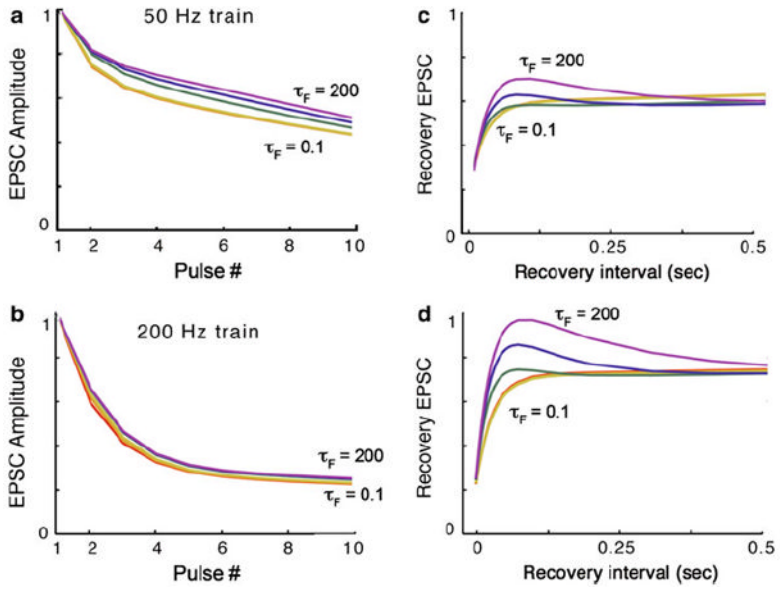

Fig. 6.

Facilitation can introduce a non-monotonic 'bump' to the recovery trajectory and faster early recovery. Model output with parametric variation of facilitation during train responses (**a,b**) and during recovery (**c,d**). All model parameters as in Fig. 5, except facilitation was added with manipulation of parameters that enhance the fraction of release with each action potential. For these curves, δ_F was fixed at 0.1, while the time constant of facilitation (τ_F) was varied from 0.1ms (negligible facilitation) to 200ms (prolonged facilitation)

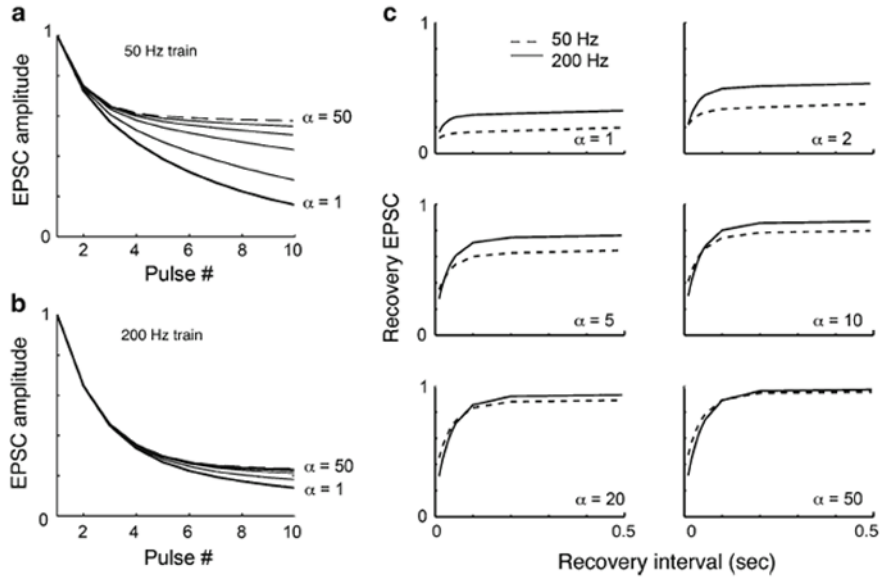

Fig. 7.

Relative pool size (α) affects the time course of recovery and the crossover effect. Model output with parametric variation of α during train responses (**a,b**) and during recovery (**c**). An α of 1 means the pool sizes in the model were equal; α of 50 means the backup pool size is 50 × larger than the ready-releasable pool. The plots in **c** compare the recovery curves following the 50 Hz stimulus (*dashed lines*) and 200 Hz stimulus (*solid line*). When α is low, recovery is dominated by the slow time constant (*top left* in **c**). When α is high, the crossover is nearly eliminated, but recovery is dominated by fast time constant

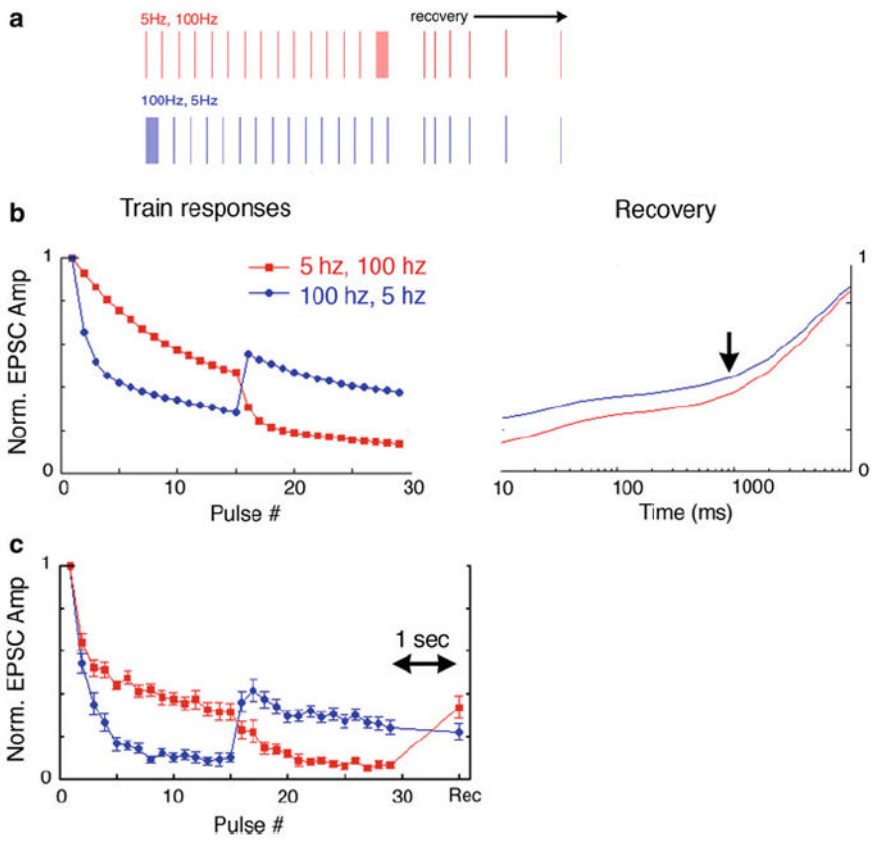

Fig. 8.

Combination trains distinguish the cascade model from other activity-dependent models Stimulation trains consisted of two blocks of pulses at 5Hz followed by 100Hz or vice versa (**a**). Recovery of the EPSC is probed at varying intervals following the end of the trains. **b** Model prediction of EPSC amplitudes during the train (*left panel*) and the recovery trajectory following the end of the trains. Note that the trajectory following the 5Hz/100Hz train (*red*) never exceeds the trajectory following the 100 Hz/5Hz train (*blue*). Model parameters as in Fig. 5. **c** Experimental test of the model showed that the data during the trains closely followed the model, but the recovery measured at 1 s showed a clear crossover